H1-5/00-582
PRC-01/00

Proposal for Installation of a Very Forward Proton Spectrometer in H1 after 2000

L. Favart, D. Johnson, P. Marage, R. Roosen,

Inter-University Institute for High Energies ULB-VUB, Brussels, Belgium

E.A. De Wolf, P. Van Mechelen, T. Anthonis

Universitaire Instelling Antwerpen, Wilrijk, Belgium

L. Jönsson, H. Jung,

Physics Department, University of Lund, Lund, Sweden

V. Blobel, F. Büsser, V. Jemanov, A. Meyer, B. Naroska, F. Niebergall, J. Schütt, H. Spitzer, R. vanStaa

University Hamburg II Institut f. Experimentalphysik, Hamburg, Germany

P.R. Newman,

School of Physics and Space Research, University of Birmingham, Birmingham, UK

Abstract

A new, very forward proton spectrometer (VFPS) with large acceptance is proposed to be installed in the proton beam of the H1 experiment after the luminosity upgrade in the year 2000. The spectrometer, located at 220 m downstream of the interaction point is based on the Roman Pot technique and consists of two stations situated in the cold section of the proton beam line. The proposal presents the physics motivations, a description the proton spectrometer, a technical solution for the installation in the cold beam section, a cost estimate and time planning.

Contents

1 Introduction

Diffractive physics has received in recent years considerable interest, from the experimental side as well as from theory. Important information has been obtained by the HERA experiments, leading to considerable progress in the partonic interpretations of diffraction. However, the understanding of diffraction in terms of QCD is still particularly challenging, and various very different models are broadly compatible with the existing data. Discriminating between these models and further progress in the field will depend directly on collecting large statistics of high quality experimental data, in various inclusive, semi-inclusive and exclusive channels.

Most experimental results have been obtained so far at HERA using events characterised by the presence of a large gap in rapidity between final state hadrons, without the direct tagging of the scattered proton. However, experimentally, the most precise and unambiguous way of studying diffraction is by measuring directly the scattered proton four-momentum, by means of a proton spectrometer. Such devices have been installed by the H1 and ZEUS collaborations, and have delivered interesting results, but their acceptance is small and the collected statistics are limited.

To extract high quality data and take full advantage of the luminosity increase at HERA after the year 2000 [1], a very forward proton spectrometer (VFPS) which measures the diffracted proton with a very good acceptance is thus essential. In this note we propose the installation of a system of two $\mathrm{Roman\ pots}$, equipped with scintillating fibre detectors, in the cold section of the proton beam line, 220 m downstream of the H1 main detector. Using beam transport calculations based on the new HERA optics, the expected performance of the proposed VFPS is quantified.

An essential feature of the present proposal is the very high acceptance expected for the spectrometer in the proposed location, for the full range in t, the four-momentum transfer squared of the incident proton to the scattered proton. Large statistics can thus be accumulated and uncertainties related to extrapolations in t are avoided. Still more important, the experimental error due to the uncertainty on the precise positioning of the pots in the course of data taking is avoided, in contrast with the case where the acceptance strongly varies with t.

In the present note, we first review in section 2 the major physics issues which could be addressed with this new device after the luminosity upgrade. In section 3, a comparison is made between the existing FPS and the VFPS. The expected acceptance and resolution for the selected position of the VFPS are discussed in section 4 and 5 . The proposed modifications to the cold section of the proton beam line are addressed in section 6. The Roman pot detectors are presented in section 7 and 8 including the data acquisition and electronics. Preliminary cost estimates, time planning and sharing of responsibilities between participating institutes are given in section 9.

2 Physics Issues

2.1 Diffraction at HERA: Present Status

With the considerable amount of experimental results on diffractive processes, collected since 1993 at HERA, the understanding of diffraction has substantially progressed with the focus

gradually moving from aspects related to inclusive properties of diffraction towards processes which are marked by the presence of a "hard" scale.

The measurement of a diffractive structure function $F_2^{D(3)}\left(Q^2,\, x,\, x_{I\!P}\right)$ [1] has led to the important result that the energy dependence of diffractive photon dissociation in the deep inelastic domain is stronger than the one obtained from "soft" hadron−hadron processes. From this measurement, using QCD evolution, parton distributions in the pomeron were extracted which indicate that the pomeron is dominated by gluons.

Several studies regarding semi-inclusive features of the hadronic final state in diffractive deep-inelastic scattering have been performed: event shape [4, 5], multiplicity distributions [6], energy flow and single particle spectra [5, 7]. Almost all of these final state characteristics are in qualitative agreement with model predictions based on the parton distributions in the pomeron extracted from the inclusive measurements, indicating that these parton distributions universally describe diffractive DIS observables.

Of particular importance, in connection with QCD predictions, are the measurements performed on those diffractive final states which exhibit the presence of a hard scale: diffractive dijet production (both in photo- and in electroproduction) [8, 9] and diffractive charm production (via the $D^* \to D\pi \to K\pi\pi$ production) [10, 11].

Finally, diffractive vector meson production has been measured in quite some detail. Most important here is the observation of a fast rise of the heavy quark cross section with energy (J/ψ photo- and electroproduction) and, possibly, a similar behaviour at large Q^2 in the ρ electroproduction channel.

These first generation experiments at HERA have thus led to important observations and conclusions concerning diffraction: transition from a "soft" to a "hard" behaviour with increasing hard scales, gluon dominance in the pomeron, consistency with the DGLAP evolution of parton distributions. The presence of a hard scale in the final state allowed more detailed QCD predictions to be verified. However, the quality of these mesurements are subject to a number of limitations. Firstly, diffractive interactions have typically been selected by the presence of a rapidity gap in the diffractive final state, but not by direct tagging of the scattered proton. Consequently, a clean separation between elastic and proton dissociation events is not possible, and a recourse to model dependent techniques is necessary to evaluate the latter contribution. Secondly, statistics are still quite limited in several channels with a manifest "hard scale". Thirdly, quantities of basic importance have still eluded measurement: a fully differential $F_2^{D(4)}$ measurement [2] and the measurement of the longitudinal diffractive cross section.

Based on this present status, we summarize below those measurements for which the proposed proton spectrometer will provide major progress in terms of high quality and high statistics data.

For the estimates on event statistics, given below, we have assumed a 20 % luminosity loss due to the VFPS operation: the VFPS can only be moved into position after stable beam conditions are reached. Hence, assuming a luminosity of 150 pb^{-1}/year, and a minimum running over 3 years (2003-2005) one can expect to collect a total effective luminosity of 360 pb^{-1}.

[1] Q^2 is the negative of the intermediate photon four-momentum squared, x is the Bjorken scaling variable and $x_{I\!P} \simeq \frac{Q^2+M_X^2}{Q^2+W^2}$ is the fraction of the proton momentum carried by the pomeron; W being the total hadronic energy of the system and M_X the hadronic mass.

[2] The Leading Proton Spectrometer in the ZEUS experiment allowed a first measurement of the t distribution, but with limited statistics and only for $|t| \gtrsim 0.1\ \mathrm{GeV}^2$.

2.2 Diffraction in the Presence of a Hard Scale

The emphasis in diffractive studies at HERA is centered on those diffractive processes which exhibit the presence of a hard scale i.e. high Q^2 values, large transverse momenta (large E_T jets), large quark mass (in particular charm production). The present statistics are limited in these kinematic regions and most analyses suffer from the presence of the proton dissociation background. A large acceptance spectrometer in the high luminosity regime after the year 2000 is thus the ideal tool for these relevant studies and would remediate the shortcomings of limited statistics and large background at the same time.

To measure well events resulting from hard scale processes, it is important to realise which $x_{I\!P}$ range is relevant. In the production of charm or jets, the diffractive mass M_X is relatively large, corresponding to small β values ($\beta = x/x_{I\!P}$). For jets with $E_T > 5$ GeV, M_X is constrained to be larger than 10 GeV. Hence, for typical W values of the order of 150 GeV, this value of M_X or larger, corresponds to $x_{I\!P} \geq 0.005$. As will be shown in section 4 this corresponds precisely to the lower acceptance limit which at that point reaches 50% and rises quickly with increasing $x_{I\!P}$ values.

It should also be emphasized that there is a lower limit to the measurement of $x_{I\!P}$ from the background point of view. The "coasting beam", i.e. beam particles traveling outside the right beam bucket and not scraped by the collimators, can have a momentum of 1 promille of the beam energy, and therefore would represent a serious background for the VFPS.

Deeply Virtual Compton Scattering and Vector Meson Production

Deeply virtual Compton scattering (DVCS) and vector meson production ($\rho, \phi, \rho', J/\psi, \psi', ...$) at high Q^2, high t or with a large quark mass are very clean diffractive channels for a QCD analysis. In both cases, the kinematics are overconstrained, leading to well reconstructed variables while the model uncertainties are minimal, in particular for the DVCS process where no uncertainty from a vector meson wave function is present. For vector meson production the Q^2-evolution can be studied in detail. Interesting results have been obtained but significant improvements are awaited, both in statistics and in systematic uncertainties. Removing the contribution of the proton dissociation background at large t is essential for reducing the present uncertainties.

Monte Carlo estimates indicate that the expected number of DVCS events to be collected with $Q^2 > 8$ GeV^2 amounts to 7000.

High E_T Jet Production

Of basic importance are the measurements of diffractive high E_T jet production, which test directly the gluon content of the pomeron and the dynamics of diffraction.

In particular, the differential distributions in diffractive jet electroproduction should enable a discrimination between basic models such as the resolved pomeron and two gluon exchange model [15]. It is estimated that the number of expected DIS events with $p_T > 5$ GeV, $Q^2 > 7.5$ GeV^2 and $0.1 < y < 0.7$ [9] amount to $\approx 10,000$ dijets. With these statistics it would

become possible to estimate the higher order contributions, like the resolved virtual photon contributions which are also non-ordered p_T emissions (as in the two gluon exchange model), by studying the z-distribution [3] (see fig 1) and to shed further light on the problem of "gap survival" probability (see below).

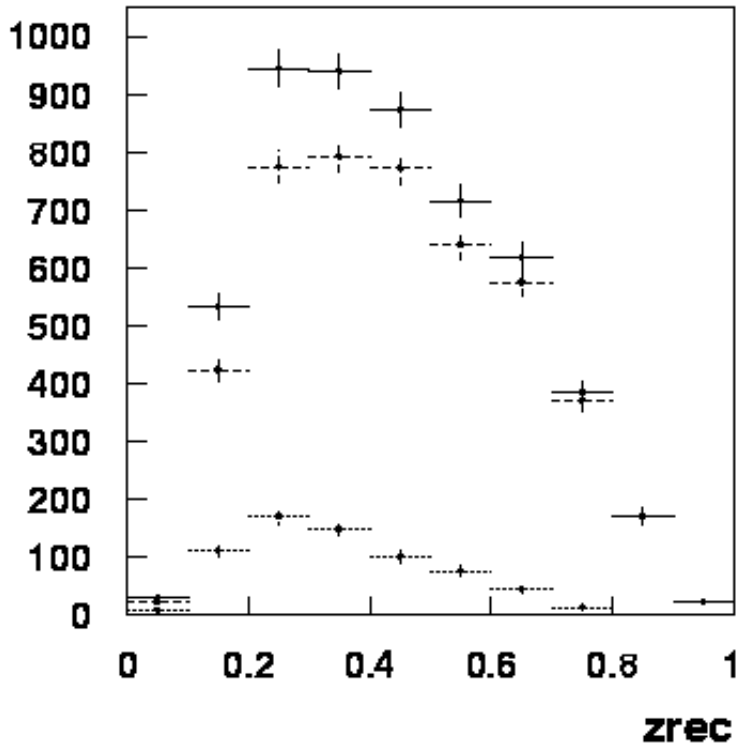

Figure 1: z-distribution for DIS jets events: direct contribution(dashed line), resolved contribution(dotted line) and sum (full line)

In photoproduction, we expect about 60 k events (presently ~ 1 k) for which $p_T \geq 5$ GeV. Due to the large statistics, the comparison of the rates for diffractive jet production by direct ($x_\gamma \gtrsim 0.8$) and resolved photons ($x_\gamma \lesssim 0.8$; x_γ is the fraction of the photon momentum entering the hard subprocess), will permit investigation of the possible mechanisms which destroy the rapidity gap ("gap survival probability" [16]). Such mechanisms would result in a lower diffractive rate for resolved than for direct photons and provide an explanation for the apparent discrepancy between diffractive production rates at HERA and at the Tevatron [17]. Clearly, these studies are of major importance for understanding diffraction in DIS at HERA and at hadron colliders.

Open Charm Production

The study of diffractive charm production provides another way of accessing directly the gluon content of the pomeron, since charm is expected to be produced mainly through the boson gluon fusion process. Different predictions have been made by several authors concerning the amount of diffractive charm production and the differential distributions. Up to now, only a

[3] $z = (M_{JJ}^2 + Q^2)/(M_X^2 + Q^2)$, where M_{JJ} is the jet-jet invariant mass; z is the fraction of the pomeron momentum carried by the parton entering the hard sub-process.

Channel	Present statistics $\rightarrow 2000$	Expected (2003-2005)
$ep \rightarrow D^{*\pm} + XN$	$\approx 100\ (55\ \mathrm{pb}^{-1})$	650

Table 1: Event statistics : $0.001 < x_{I\!P} < 0.04$

Process	Events all z	Events $z > 0.6$
Resolved pomeron	410	60
2 gluon exchange	80	32

Table 2: Charm process composition: $0.005 < x_{I\!P} < 0.03$

very limited number of charm events have been collected at HERA (a few tens of events). As shown in table 1, the expected amount of charm events to be collected by the VFPS will increase sixfold. Furthermore, restricting the $x_{I\!P}$ range to the interval $[5.\ 10^{-3}, 3.\ 10^{-2}]$ i.e. to the truly diffractive region ($\approx$ 400 events), would still allow a measurement of the charm diffractive production cross section with a 5% error. Although more statistics are needed to disentangle the resolved pomeron - two gluon exchange mechanism in the production of charm using the ϕ asymmetry [18]. More insight could be obtained on the charm production mechanism via the information of the z-distribution, as shown in the table 2.

2.3 Inclusive Measurements

2.3.1 $F_2^{D(4)}$ Measurement

Measurements on $F_2^{D(3)}\,(Q^2,\, x,\, x_{I\!P})$ have been performed by the H1 and ZEUS experiments using data taken in 1994 and 1995, and new results, based on more recent data, will become available soon. However, proton elastic events are not tagged unambiguously, leading to uncertainties related to the presence of proton dissociation backgrounds (see also section 2.4). On the other hand, the measurements performed using the present Roman pot systems of ZEUS and H1, provide only limited statistics and an acceptance which does not extend below $|t| = 0.1$ GeV^2, whereas with the proposed VFPS, the fully differential $F_2^{D(4)}\,(Q^2,\, x,\, x_{I\!P},\, t)$ diffractive structure function will be measured, down to the lowest values of $|t|$.

The $F_2^{D(4)}\,(Q^2,\, x,\, x_{I\!P},\, t)$ measurements will be performed in the purely diffractive region with $x_{I\!P} < 0.01$, where the contribution from meson exchange is negligible. The Q^2 and x variables will be measured using the main H1 detector. The $x_{I\!P}$ variable will be determined from the VFPS measurements but also, for those events for which the final state is well contained, ($x_{I\!P} < 0.01$), from measurements using the main H1 detector. Combination of these two measurements will lead to improved precision on the $x_{I\!P}$ measurement. Finally, the t variable will be directly measured by the VFPS. As shown by the studies in section 4, the lowest $|t|$ values can be measured with nearly 100% acceptance, and the resolution in t will allow the measurement of 3 or 4 data points for $|t|$ between 0. and 0.6 GeV^2. This precision will provide a handle on possible new features related to the t dependence of the cross section.

2.3.2 Longitudinal Cross Section

QCD models (see e.g. [12]) predict a dominance of the longitudinal photon induced cross section in diffraction at large β values and small to moderate Q^2. In such models, the transverse

photon contributions are of a leading twist nature and are expected to follow the DGLAP evolution equations. In contrast, large higher twist contributions are expected for longitudinal photons, leading to an unprecedented dominance of higher twist longitudinal σ_L^D over leading twist transverse σ_T^D contributions for $\beta \gtrsim 0.8$ at low Q^2. The dominance of the longitudinal cross section has been demonstrated in exclusive vector meson production for $Q^2 \gtrsim 2-3$ GeV^2 but has never been measured in the inclusive diffractive data sample; indications for the presence of a higher twist contribution have been obtained from global fits [12]. The measurement of the diffractive longitudinal structure function and the confirmation of its higher twist nature should provide decisive tests of QCD predictions, and distinguish between several related models (see review [13]).

In principle, a measurement of the longitudinal structure function requires data taken at two different beam energies at least. However, following the method proposed in [14], information can still be obtained from a single beam energy measurement using the azimuthal measurement of the scattered proton. The method relies on the dependence of the differential diffractive cross section, on the angle ϕ between the electron scattering plane and the proton scattering plane. The interference between the longitudinal and transverse amplitudes is predicted to give a modulation of the diffractive cross section proportional to $\cos\phi$, a variation which, depending on the model, can be of the order of $15-25$ % for $\beta > 0.8$. The effect is predicted to depend on Q^2 and β.

This measurement thus requires the determination of the scattered proton direction. As shown below (section 5.3), in spite of the beam dispersion and the uncertainty in the measurement of $x_{I\!P}$ (which affect the resolution), the angle ϕ is expected to be measured by the VFPS with a precision sufficient to allow for the measurement of 4 to 5 data points, for $0.1 < |t| < 0.6$ GeV^2 (for smaller $|t|$ values, ϕ cannot be determined).

2.4 Single and Double Diffractive Dissociation

Absolute Cross Section Measurements

Except for the low statistics of events accumulated with the present proton spectrometers, the H1 and ZEUS experiments have up to now not been able to isolate pure samples of events with single diffraction (elastic events). In H1, the forward detectors which detect particles with a pseudorapidity up to $\eta \approx 7$ in the laboratory frame, are used to reject proton dissociation events for which the mass of the scattered baryonic state M_Y satisfies $M_Y \gtrsim 1.6$ GeV. The remaining contamination of proton dissociation events in the elastic sample is estimated to be of the order of 10%. For ZEUS, where only the central components of the detector are typically used, the contamination is still larger ($31 \pm 15\%$ [2]). These contaminations imply significant systematic errors which affect the absolute value of the cross section for all types of measurements.

Differential Distributions; Shrinkage

The proton dissociation contamination also leads to large uncertainties in differential distributions, which can differ for elastic and proton dissociation events. A very important case is the "shrinkage" of the forward diffractive peak, i.e. the increase of the exponential slope parameter b of the t distribution with increasing energy. Shrinkage is predicted by Regge theory

for "soft" interactions, and has been observed for hadron−hadron scattering and in light vector meson photoproduction. In contrast, only very small shrinkage is predicted by QCD based models. The possible evolution of shrinkage as a function of a hard scale can thus provide precious information on the interplay between "soft" and "hard" diffraction, and is eagerly awaited. However, the b parameters for elastic and proton dissociation events differ by approximately a factor 2, and the presence of a proton dissociation background in the "elastic" sample is thus the source of a very large uncertainty. Independently of the possibility of measuring directly the t distribution, the use of a proton spectrometer which tags the diffractive proton is thus essential to measure this crucial effect.

Factorisation Breaking

More generally, the present analyses rely on a "factorisation hypothesis", for which no direct experimental support exists in the presence of a hard scale, and which is at variance with several QCD predictions. This hypothesis states that the distributions which are not directly related to the scattered baryonic state Y, i.e. the distributions related to the scattered electron and the system X, are the same for elastic and proton dissociation interactions. This hypothesis is directly relevant for the $F_2^{D(3)}$ measurements, and thus for the extraction of parton distributions, as well as for all final state analyses, including jet, charm and vector meson production. In particular, this hypothesis is tacitly assumed when comparisons are performed between results from H1 and ZEUS, which have different levels of proton dissociation contamination. It is also tacitly assumed in all comparisons between experimental results and theoretical predictions computed for elastic proton scattering. The use of a proton spectrometer with a high acceptance, independent of t, is the only experimental means to avoid this factorisation assumption.

Study of Proton Dissociation

Conversely, the use of a proton spectrometer will facilitate measurements of the proton dissociation process in the crucial region of the proton excitation mass $1.6 \lesssim M_Y \lesssim 15\,\mathrm{GeV}$. The proton dissociation sample can be obtained by the subtraction of the tagged elastic contribution from the full (elastic + proton dissociation) diffractive event sample, selected by the observation of a rapidity gap in the main detector. As mentioned, a breaking of factorisation is expected in QCD. A study of possible factorisation breaking effects increasing in the presence of a hard scale is thus another means of accessing information on the interplay between "soft" and "hard" diffraction.

2.5 Conclusions

$\mathrm{Roman\ pots}$ with large acceptance, down to very small $|t|$ values, provide a decisive improvement compared to the first generation of diffractive experiments at HERA. A clean measurement of truly elastic events is possible, by the direct tagging of the scattered proton, avoiding the systematic uncertainties due to the remaining contamination of proton dissociation events. This will facilitate the precision measurement of the $F_2^{D(3)}$ diffractive structure function, as well as the accumulation of large event samples with a hard scale after the luminosity upgrade. The use of a proton spectrometer will permit the measurement of the $F_2^{D(4)}$ structure function, with a good precision in t. It will provide extremely important information at large β values on the longitudinal diffractive structure function, expected to be of a higher twist nature. It will make possible the study of shrinkage and of factorisation breaking effects between single and double dissociation, thus providing information on the interplay between soft and hard diffraction.

3 Existing FPS versus New VFPS

After the luminosity upgrade the existing FPS will still be operational in H1. In order to demonstrate the complementary behaviour of the two spectrometers, Fig. 2 shows the acceptance of the horizontal and vertical existing pots and of the new VFPS at 220 m as a function of $x_{I\!P}$. Fig. 2 clearly shows that, although the existing FPS can measure $x_{I\!P}$ down to 10^{-4}, its acceptance is very small in contrast to the VFPS. Together with the vertical FPS pots an $x_{I\!P}$ range of $[5.10^{-3}, 10^{-1}]$ will be covered with very good acceptance.

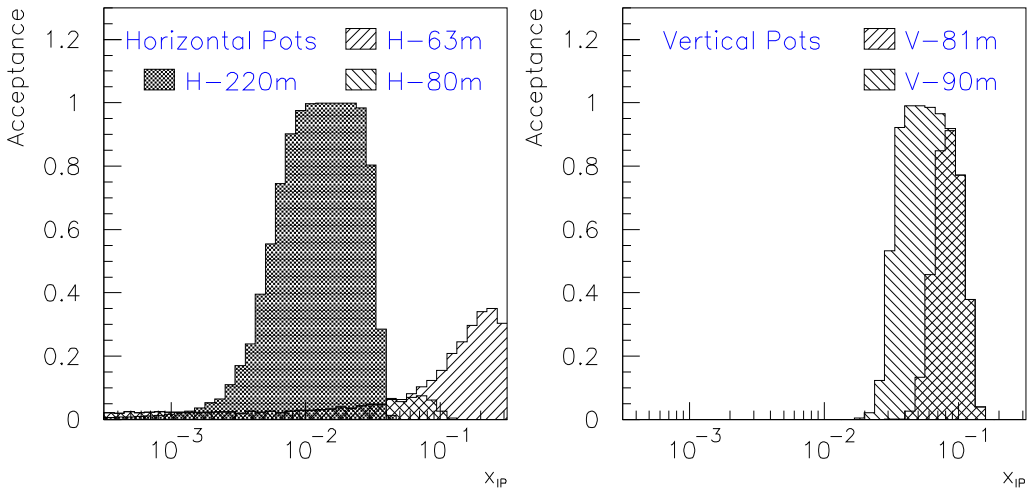

Figure 2: Acceptance of the FPS as a function of $x_{I\!P}$ for the vertical and horizontal stations respectively.

4 Proton Spectrometer Layout

The proton spectrometer (VFPS) consists of a set of two "Roman pots ". The Roman pot principle is based on the construction of an insert into the beam pipe which allows tracking detectors to be moved very close to the beam (in the present case the movement is horizontal). The insert (plunger vessel) and detectors can be moved in and out of the beam by means of mechanical gears, the detectors being operated at atmospheric pressure. The Roman pots are retracted during injection and beam dump, and are, during stable beam conditions, moved to a position as close as possible to the beam whilst ensuring that the particle rate in the detectors is not too high and the presence of the Roman pots does not limit the beam lifetime.

The strong spectroscopic effect of the horizontal HERA bend, which starts around 130 m downstream of the H1 interaction point, can be exploited to measure protons arising from diffractive interactions with a very high acceptance at low $x_{I\!P}$, independent of $|t|$.

4.1 Trajectory Simulation

In order to determine the optimal detector location as well as its acceptance, the HERA beam optics, corresponding to the high luminosity post-2000 scheme, have been simulated using a

beam transport matrix calculation in the Linear Beam Optics approximation.

The beam optics are described by the amplitude function $\beta(s)$, the inclination of the phase ellipse $\alpha(s) = -\frac{1}{2}\mathrm{d}\beta/\mathrm{d}s$, the dispersion function $D(s)$ and the beam emittance ϵ. The variable s corresponds to the position along the proton beam line of a proton ($s = s_0 = 0$ at the H1 nominal interaction point). In this description of the beam parameters, a local coordinate system is adopted: the x-axis points to the center of the HERA ring and measures the horizontal deviation of the particle trajectory with respect to the nominal beam position; the y-axis points vertically upward and measures the vertical deviation. The profile of the circulating beam is assumed to be Gaussian. Its width ("beam envelope") is given by : $\sigma_x(s) = \sqrt{\epsilon_x \beta_x(s)}$ and $\sigma_y(s) = \sqrt{\epsilon_y \beta_y(s)}$.

The position x, the slope $x' = \mathrm{d}x/\mathrm{d}s$ and the particle energy loss $\xi = (E_{nominal} - E)/E_{nominal}$ at any position s along the beam line are related to the same quantities at the interaction point through the matrix equation :

$$\begin{pmatrix} x(s) \\ x'(s) \\ \xi \end{pmatrix} = \begin{pmatrix} T_x^{11}(s_0,s) & T_x^{12}(s_0,s) & D_x(s_0,s) \\ T_x^{21}(s_0,s) & T_x^{22}(s_0,s) & D'_x(s_0,s) \\ 0 & 0 & 1 \end{pmatrix} \cdot \left[\begin{pmatrix} x_0 \\ x'_0 \\ \xi_0 \end{pmatrix} + \begin{pmatrix} 0 \\ \theta_x \\ x_{I\!P} \end{pmatrix} \right]. \quad (1)$$

where T_x^{ij} is the beam transport matrix projection onto the x axis (a similar equation holds for the vertical plane).

The projections of the proton polar scattering angle along the x and y axis, θ_x and θ_y, are related to t and to the proton beam energy, E_p, by:

$$|t| = (1 - x_{I\!P})\, E_p^2\, (\theta_x^2 + \theta_y^2). \quad (2)$$

The values of the beam parameters for the HERA-2000 beam are given in Table 3 ([19].

	$s = 0$ m	$s = 220$ m
β_x	2.45 m	31.7 m
β_y	0.18 m	104.1 m
α_x	0.0	-2.1
α_y	0.02	3.0
Dx	-0.1 mm	1045.0 mm
$D'x$	-3.3 mRad	22.3 mRad
Dy	-0.1 mm	2.4 mm
$D'y$	-1.4 mRad	-0.1 mRad
$\epsilon_x = \epsilon_y$	$5.66 \cdot 10^{-9}$ m	

Table 3: HERA-2000 main beam parameters at the interaction point and at the $\mathrm{Roman\ pot}$ installation location.

In order to estimate the $\mathrm{Roman\ pot}$ acceptances, we have calculated the projected x and y beam contours corresponding to 12 times the beam envelopes (σ_x, σ_y), shown in Fig. 3. The

12 σ "distance" is expected to be a position where the detectors are not exposed to excessive beam rates. The beam energy loss was set to a fixed value, corresponding to $x_{I\!P} = 10^{-2}$ ($x_{I\!P} = 1 - E_{p'}/E_p$), while for $|t|$ three different values have been assumed, 0.5, 0.1 and $0.01\ \mathrm{GeV}^2$. The difference in the beam contours corresponding to the different values of $|t|$ are shown in Fig. 3 by the colour shaded areas. For this calculation, a detailed description of the future beam pipe size was not taken into account: we have assumed that the scattered proton trajectories encounter no obstacles in a plane transverse to the beam within the 12 σ boundary, up to 80 m; from there onward, a fixed transverse distance of 5.5 cm is assumed.

4.2 Detector Position along the Beam Line and Acceptance

The results in Fig. 3 show that scattered protons with $x_{I\!P} = 10^{-2}$ and $|t| \leq 0.1\ \mathrm{GeV}^2$ leave the 12 σ beam envelope at locations beyond 160 m, and hence can be tagged. Between 160 m and 250 m downstream of the H1 interaction point, there exist three drift spaces large enough to install a set of two $\mathrm{Roman\ pot}$ detectors. These drift spaces are located in the intervals $[158.0,\ 171.5]$ m, $[185.3,\ 196.9]$ m and $[214.9,\ 225.3]$ m. At a distance further removed from the interaction point, the structure of the proton beam line magnets changes and no large drift spaces are present.

Calculations show that, in the three possible drift spaces, the resolutions for measurements in t and ϕ of the diffracted proton are comparable, but the acceptance is largest at the $[214.9,\ 225.3]$ m position. Therefore only this location is considered below and will be refered to as the 220 m location.

At a given position along the proton beam line, the spectroscopic effect of the beam magnets is such that scattered protons with larger $x_{I\!P}$ values, i.e. larger energy loss, are more strongly bent in the transverse plane than those at lower $x_{I\!P}$ (see the insert of Fig. 4). The result is that the impact point of scattered protons produced at a scattering angle $\theta = 0$ is translated in the (x, y) plane, and this shift is a measure of $x_{I\!P}$. As a result of the variation in the position of the interaction point x_0, y_0, the beam divergence x_0', y_0' and the beam energy dispersion ξ_0 ($\xi_0 = 6.10^{-5}$) at s_0, this shifted impact point will furthermore be smeared. In addition, the initial transverse momentum ($p_T^2 \simeq |t|$) of the scattered proton gives a contribution to the position of the impact point in the transverse plane. The combined effect, for a diffracted proton with $x_{I\!P} = 10^{-2}$ and $0 < |t| < 0.5\ \mathrm{GeV}^2$ is shown in Fig. 4. The 12 σ beam contour is also shown.

To evaluate the dependence of the detector acceptance on the distance of approach to the proton beam, we have calculated the acceptance for detector positions corresponding to 10, 15 and 20 times the beam envelope. In order to simulate the dead material between the active detector region and the beam edge due to the plunger vessel walls we have retracted the detectors an extra 300 μm from the nominal beam line in the simulation. Fig. 5 shows the acceptance as a function of $x_{I\!P}$ and $|t|$. The t integrated acceptance as a function of $x_{I\!P}$, using a weight factor of $e^{7.t}$, assuming a 12 σ beam approach, is shown in Fig. 6. The $|t|$-dependence of the acceptance is shown in Fig. 7 for three different values of $x_{I\!P}$. An acceptance exceeding the 50 % level is found for scattered protons with $5.10^{-3} < x_{I\!P} < 3.10^{-2}$ and $|t| < 0.5\ \mathrm{GeV}^2$ and $\approx 100\%$ for $10^{-2} < x_{I\!P} < 3.10^{-3}$, $\mid t \mid < 0.2\ \mathrm{GeV}^2$. The acceptance limitations at large $x_{I\!P}$ and $|t|$ depend on the assumed boundaries for the inner beam pipe size, the simulation of which has been described above.

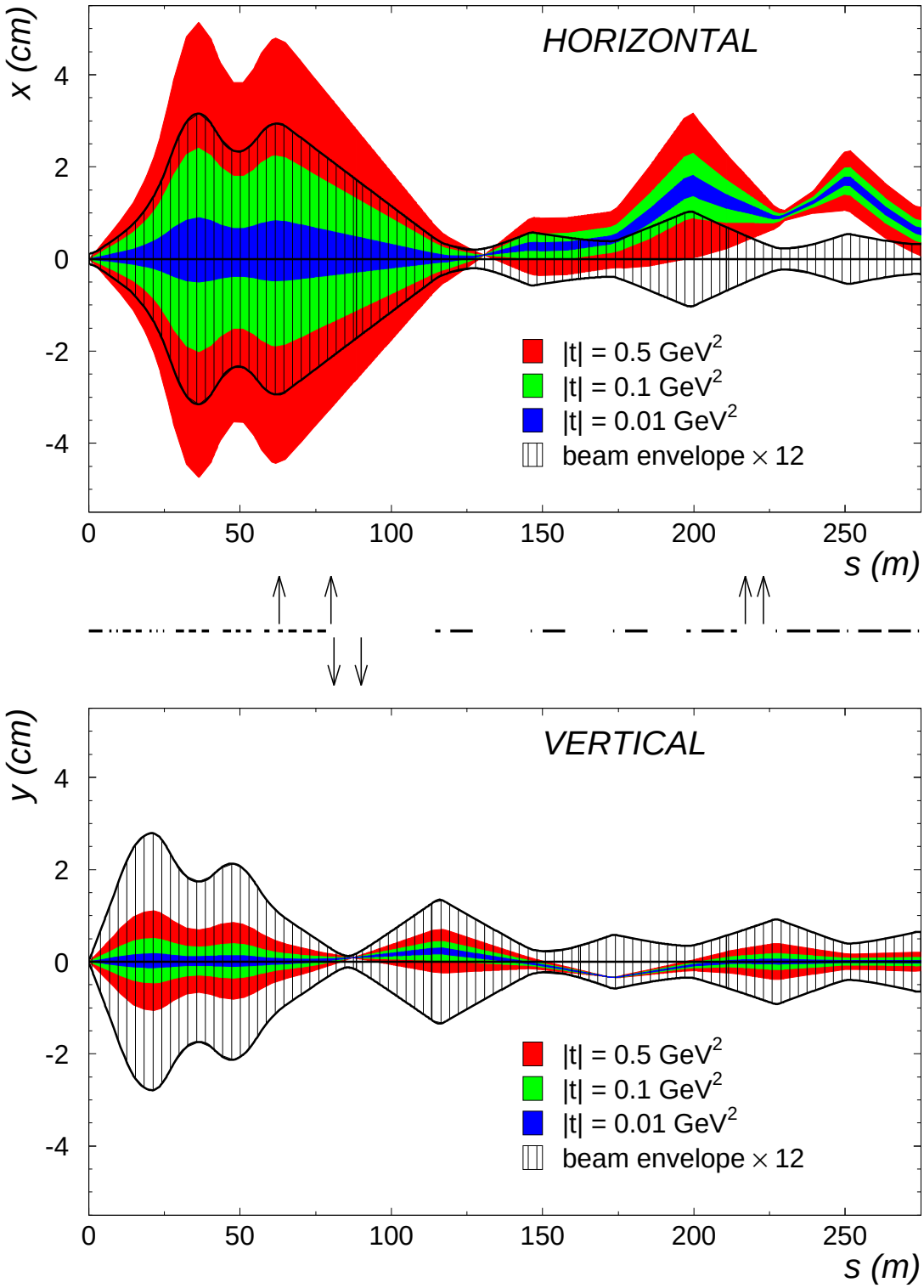

Figure 3: Horizontal and vertical projections of 12 times the beam envelope, as a function of the distance to the interaction point (hatched areas). The projection of the transverse distances of the scattered protons for three different t values and for $x_{I\!P} = 10^{-2}$ are given by the shaded areas. The horizontal dashes between the two figures indicate the locations of the magnets. The vertical arrows indicate the positions of the present FPS stations and the proposed positions for the new Roman pots .

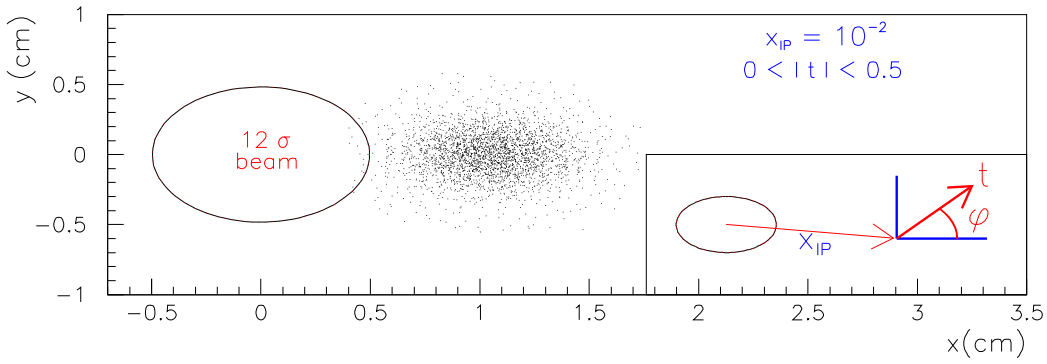

Figure 4: Spread of the impact point of diffractive protons in the (x, y) plane due to variations in initial conditions. The beam envelope (multiplied by a factor 12) is also shown. **Insert:** Illustration of the relation between the impact point of the scattered proton in the transverse plane (x, y) and the variables $x_{I\!P}$, t and ϕ.

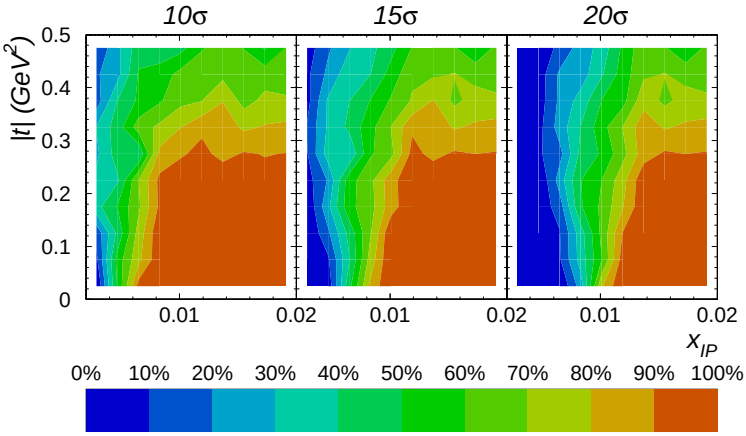

Figure 5: Acceptance of Roman pot detectors as a function of $x_{I\!P}$ and $|t|$, for an approach at 10, 15 and 20 beam envelopes.

5 Reconstruction of the Kinematical Variables - Resolutions

5.1 Principle

From the measured impact points in the two Roman pot stations, the positions (x, y) and angles (x', y') of the scattered proton at a position halfway between the two stations are determined. These in turn, are used to reconstruct the kinematics of the diffractively scattered proton, i.e. the relative energy loss, $x_{I\!P}$, and the horizontal and vertical scattering angles, θ_x and θ_y. The relation between both sets of variables is fixed by beam transport matrices as given by Eq. (1).

With four coordinate measurements and only three variables to determine, this leads in principle to an overconstrained set of equations. This set can be solved by minimizing a χ^2 expression between the actual measured coordinates and the functional expression given by Eq. 1 with respect to the kinematical variables. In practice, however, the vertical displacement

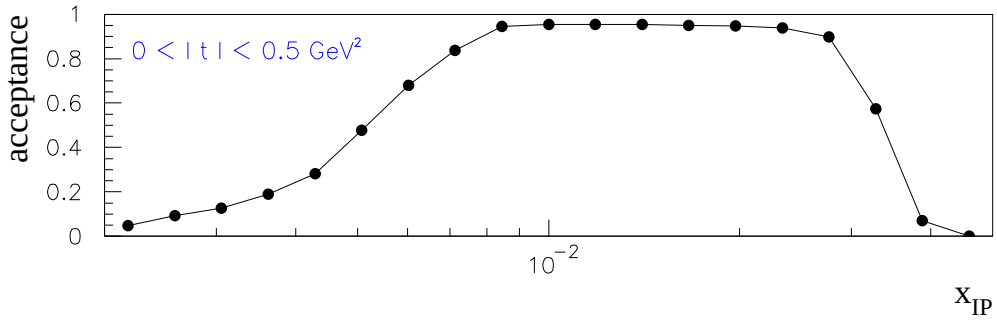

Figure 6: Acceptance of Roman pot detectors as a function of $x_{I\!P}$.

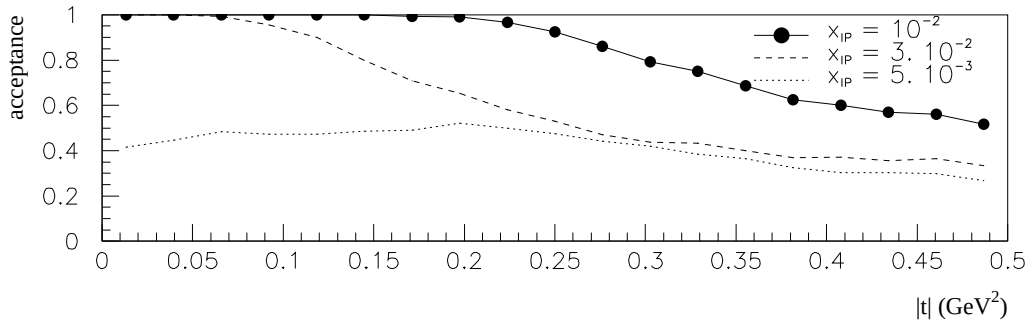

Figure 7: Acceptance of the Roman pot detectors as a function of $|t|$ for 3 different values of $x_{I\!P}$.

of the impact point of the diffractive protons resulting from a variation in $x_{I\!P}$, is negligible in the $x_{I\!P}$ range considered. Hence, $x_{I\!P}$ and θ_x are almost completely fixed by the measurements in the horizontal direction, the measurement of the vertical position is only used to determine θ_y. This is confirmed by Fig. 8, which shows the mapping of lines of constant θ_x (θ_y) and $x_{I\!P}$ in the x-x' (resp. y-y') plane. In the vertical direction all scattered protons within the acceptance range and with different $x_{I\!P}$ values are projected into a narrow region in the y-y' plane, corresponding to an almost constant $x_{I\!P}$ value.

5.2 Detector-Beam Position Calibration

To obtain accurate $|t|$ and $x_{I\!P}$ measurements, knowledge of the transverse detector positions with respect to the beam is imperative. It is therefore important to be able to determine them ("calibrate" the $|t|$, $x_{I\!P}$ measurement) from a sample of diffractive events. The effect of a transverse detector offset can be seen from consideration of Fig. 8. To calculate the detector offsets (x_0, y_0), the measurements of both the horizontal and vertical impact points are used. In the vertical direction, one degree of freedom can immediately be eliminated by requiring that all points be distributed around the single line of constant $x_{I\!P}$. The other degrees of freedom can be constrained by a combination of the following calibration methods:

- *Kinematic peak method.* As the VFPS accepts protons over the full $|t|$-range down to the lowest possible values, the measured θ-distributions are expected to peak at zero. It is

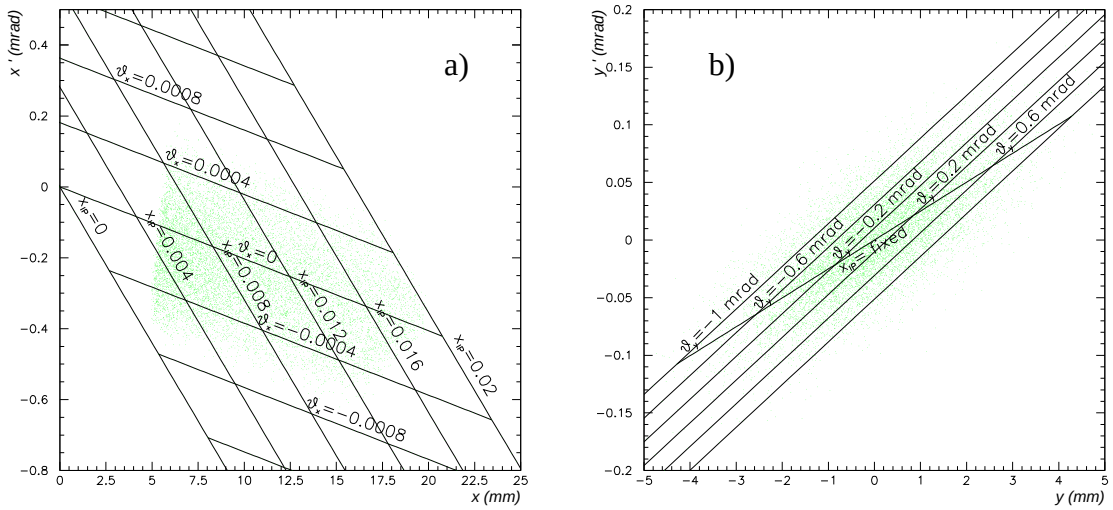

Figure 8: Lines of constant θ or $x_{I\!P}$ as a function of the proton slope and position halfway between the two $\mathrm{Roman\ pot}$ stations: a) for the horizontal direction, b) for the vertical direction. The points represent scattered protons within the VFPS acceptance.

therefore possible to use the mean value of these distributions as a calibration reference point. This constrains the movement of the measured hits in the x-x' (or y-y') plane along the lines of constant $x_{I\!P}$. The acceptance profile can distort the tails of the θ-distribution (i.e. at high $|t|$), especially in the horizontal direction. This can be minimized by selecting events in a narrow range of $x_{I\!P}$ where the acceptance is guaranteed to be nearly 100%.

- $x_{I\!P}$ *determined by the central detector.* For the $x_{I\!P}$ range considered in this proposal, a very large fraction of the diffractive events will show a rapidity gap and thus the central H1 detector is able to measure the proton energy loss with an accuracy of around 20%. This measurement can be used to fix the movement of the measured hits in the x-x' plane along the lines of constant θ_x.

- *Elastic production of ρ-mesons in the central detector.* The observation of the reaction $ep \to ep\rho$ leads to a well constrained reconstruction of the diffractive kinematics from the decay $\rho^0 \to \pi^+\pi^-$. Although these events constitute only a small subsample (≈ 200 events/proton fill) of all diffractive events, they can be used as an independent cross-check of the calibration procedure.

The position of the $\mathrm{Roman\ pot}$ relative to the beam may vary for each proton beam fill. Hence, the outlined calibration procedure is only of practical use, if the diffractive event sample, collected during a single proton beam fill, is large enough for the χ^2-method to converge. To this end, an algorithm combining the kinematic peak and the central $x_{I\!P}$ measurement has been applied using different numbers of events for the calibration, assuming one detector was displaced by 200 μm. As can be seen in Fig. 9, the algorithm determines the predefined detector offset with an accuracy compatible with the intrinsic resolution (detector, beam) from a sample of less than 200 events. For the alternative method, exploiting the observation of elastic production of ρ-mesons in the central detector, the statistics are smaller than in the kinematic peak method,

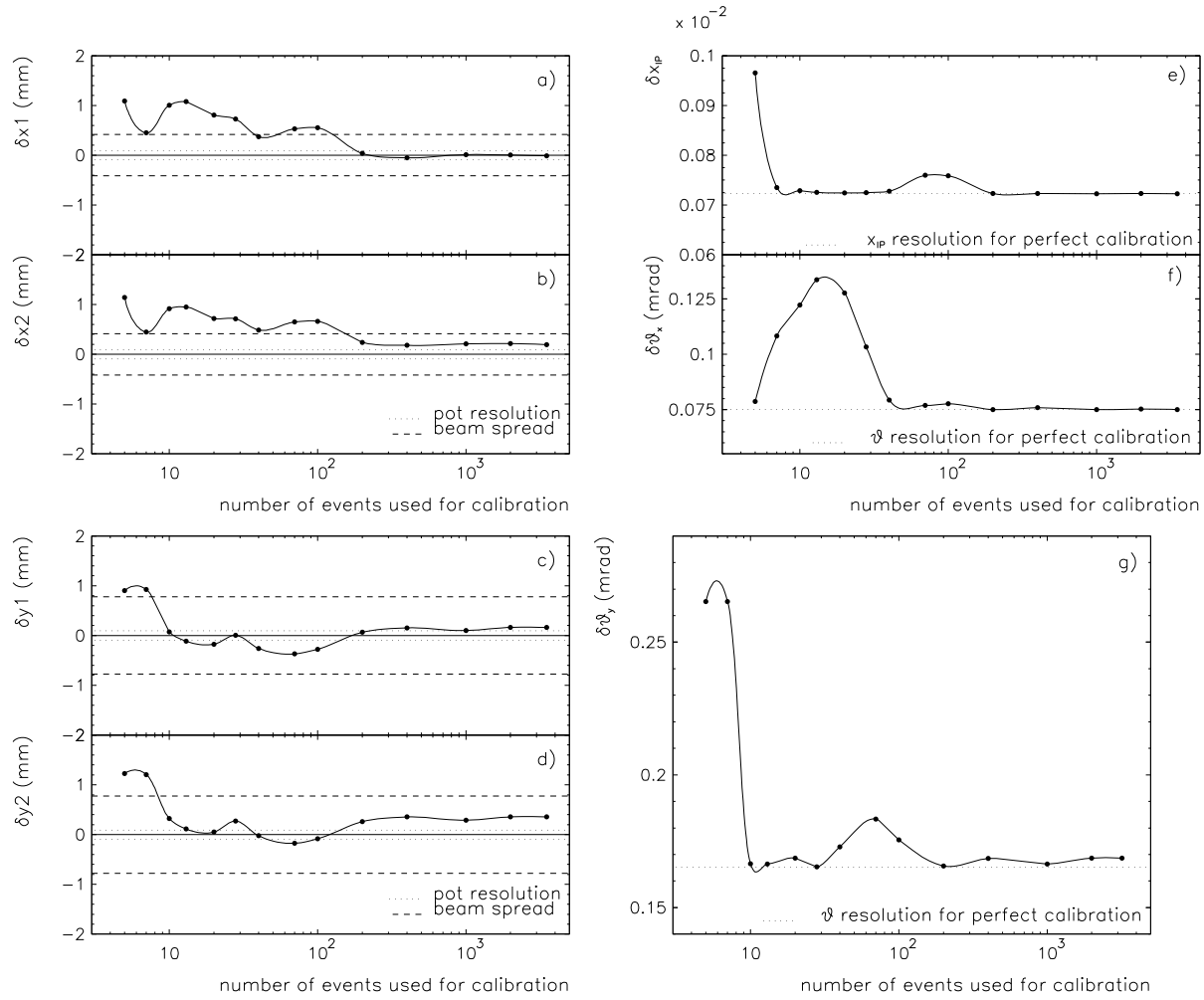

Figure 9: a-d) The reconstructed detector offsets ($\delta x1, \delta x2$) as a function of the number of events used in the algoritm. Also shown are the limiting uncertainties due to the intrinsic detector resolutions and beam divergence at the location of the $\mathrm{Roman\ pot}$ stations (dotted lines). e-g) The error on the reconstructed kinematic variables as a function of the number of events used for calibration. The errors decrease rapidly to the limited values from the intrinsic resolution.

and it therefore would be used as a cross check of the previous method using events from several proton beam fills.

5.3 Resolutions in t and ϕ

The measurement of two impact point positions, in each of the two $\mathrm{Roman\ pots}$, provides the mesurement of x, y, x' and y' which allow, using the equation (1), the reconstruction of the momentum transfer t, the momentum loss $x_{I\!P}$ and the azimuthal angle ϕ of the scattered proton.

The resolution in $x_{I\!P}$, as shown in Fig. 9.e, has a constant absolute value of 0.0075. With a spatial detector resolution of 100 $\mu\mathrm{m}$ (see section 7) the ultimate resolution on t and ϕ of the diffracted proton is determined by the intrinsic beam spread. The errors on t and ϕ are shown in Fig. 10, assuming an uncertainty in the $x_{I\!P}$ measurement of 20% [3]. The error on t

(independent of $x_{I\!P}$) varies from 0.075 to about 0.2 GeV^2 and the error on the ϕ angle varies between 0.2 to 0.8 rad (the error in ϕ increases with decreasing $|t|$ values down to $t = 0$).

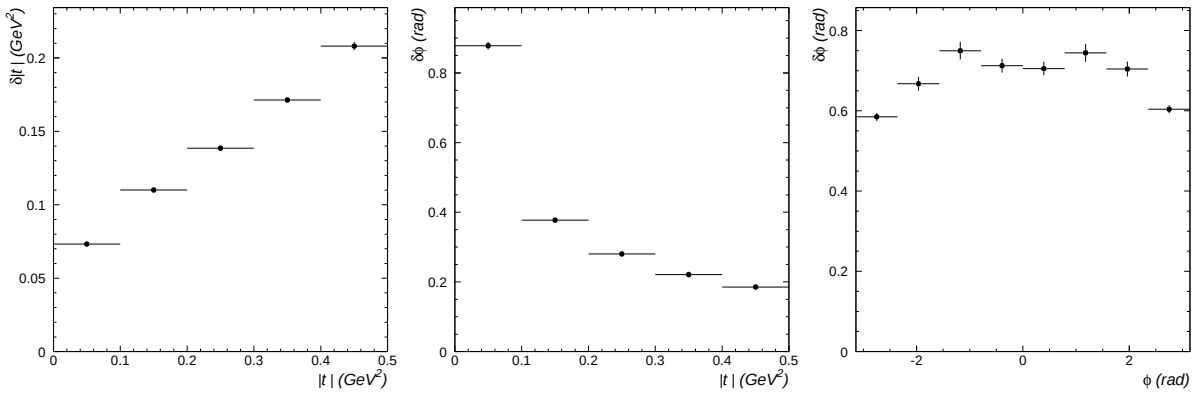

Figure 10: Errors on $|t|$ and ϕ as a function of $|t|$ and ϕ .

6 The Cold Beam Line Bypass

The Roman pots will be installed in a 6.2 m long drift section of the proton beam line located at about 220 m from the H1 experiment in the NL section of the HERA ring. This drift section belongs to the cold part of the HERA proton ring. Fig. 11 shows a cross sectional view of the drift tube at $\approx$ 220 m. As can be seen in Fig. 11 the tube contains in addition to the beam

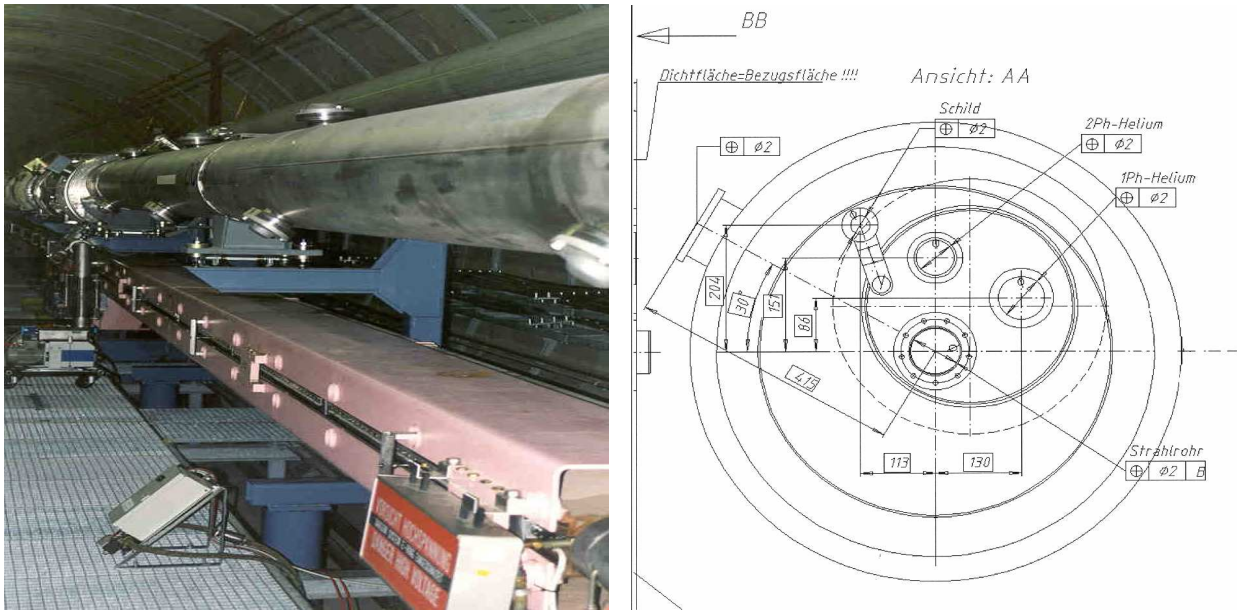

Figure 11: Left: Hera tunnel with proton (top) and electron (bottom) beam line; Right: Cross sectional view of the present drift tube at $\approx$ 220 m. The outer two circles represent the stainless steel tube. The darker circle indicates the heat shield. The 1-phase and 2-phase helium lines together with the beam pipe are encircled by a thermal heat shield which is connected to the outer heat shield.

pipe the 1-phase and 2-phase helium lines, and the whole system is contained in two successive interconnected heat shields. In order to access the beam pipe with $\mathrm{Roman\ pot}$ detectors, the proton beam line has to be "warm" i.e. at room temperature, which means a separation of the beam pipe from the cold elements of the drift tube.

A "bypass" scheme has been worked out with the DESY Cryogenics group, the Vacuum Group and an external engineering office, in which the complete drift section is replaced by a warm beam pipe and a U-turn bypass (towards the outer part of the HERA ring) which contains all cold lines. The result of this pre-study is presented in Fig. 12, which shows a horizontal and a vertical view of the bypass. The two beam pipe sections are shown as they leave the dipole and quadrupole cold sections. Two shutter valves are located at the extremities of the new beam pipe section to guarantee a shutoff of the vacuum in case of a leak. Two sets of two titanium sublimation pumps will minimize the condensation of the residual gas impurities in the cold part of the proton beam line, a leak detected via these Ti-pumps will activate the shutters. Between the two sets of pumps, two T-shaped tubes, connected to the beam pipe by bellows, form the inserts for the $\mathrm{Roman\ pots}$. The bellows compensate possible mechanical stresses in the warm/cold beam pipe.

The bypass will be assembled from several separate parts and will be transported to the HERA tunnel as a whole. The fixation and/or support of the bypass as well as the new beam tube will use the existing support structure of the present drift section with possible connections to the tunnel wall. A list of the major construction elements has been established and a first description of the mounting of the complete bypass in and outside the HERA tunnel has been made.

The cross sectional view of the HERA tunnel at $\approx$ 220 m is sketched in Fig. 13, showing the beam pipe, the bypass and the cold components as well as the electron beam and part of the support structure. Also marked on the figure is the area on the inside of the HERA ring which is to be left free for the tunnel chariot. The available space for the installation of the $\mathrm{Roman\ pot}$ detector is 1 m.

A preliminary study of the response of the proton beam R.F. system to the new beam pipe and $\mathrm{Roman\ pot}$ inserts did not reveal any definite problems. However, refined calculations with the final design of $\mathrm{Roman\ pot}$ plunger vessels are still in order.

7 Roman Pots

Many of the design aspects for the new Roman Pots, including the plunger vessel and the scintillating fibre detectors, are adaptations of the design of the FPS detectors installed and operational in H1 since 1994. However, the experience accumulated in various experiments (H1, HERA-B) as well as technical progress regarding fibres and photomultipliers have resulted in several modification with respect to the existing FPS design ([20, 21]).

A $\mathrm{Roman\ pot}$ basically consists of a plunger vessel which can be moved closely to the beam line via T-shape inserts (see Fig. 12) in the beam pipe. A connection between the beam pipe and plunger vessel realised via bellows allows a mechanical movement of the plunger vessel perpendicular to the beam line, and seals the beam pipe vacuum. The detectors installed in the plunger vessel operate at atmospheric pressure and are flushed with N_2 gas.

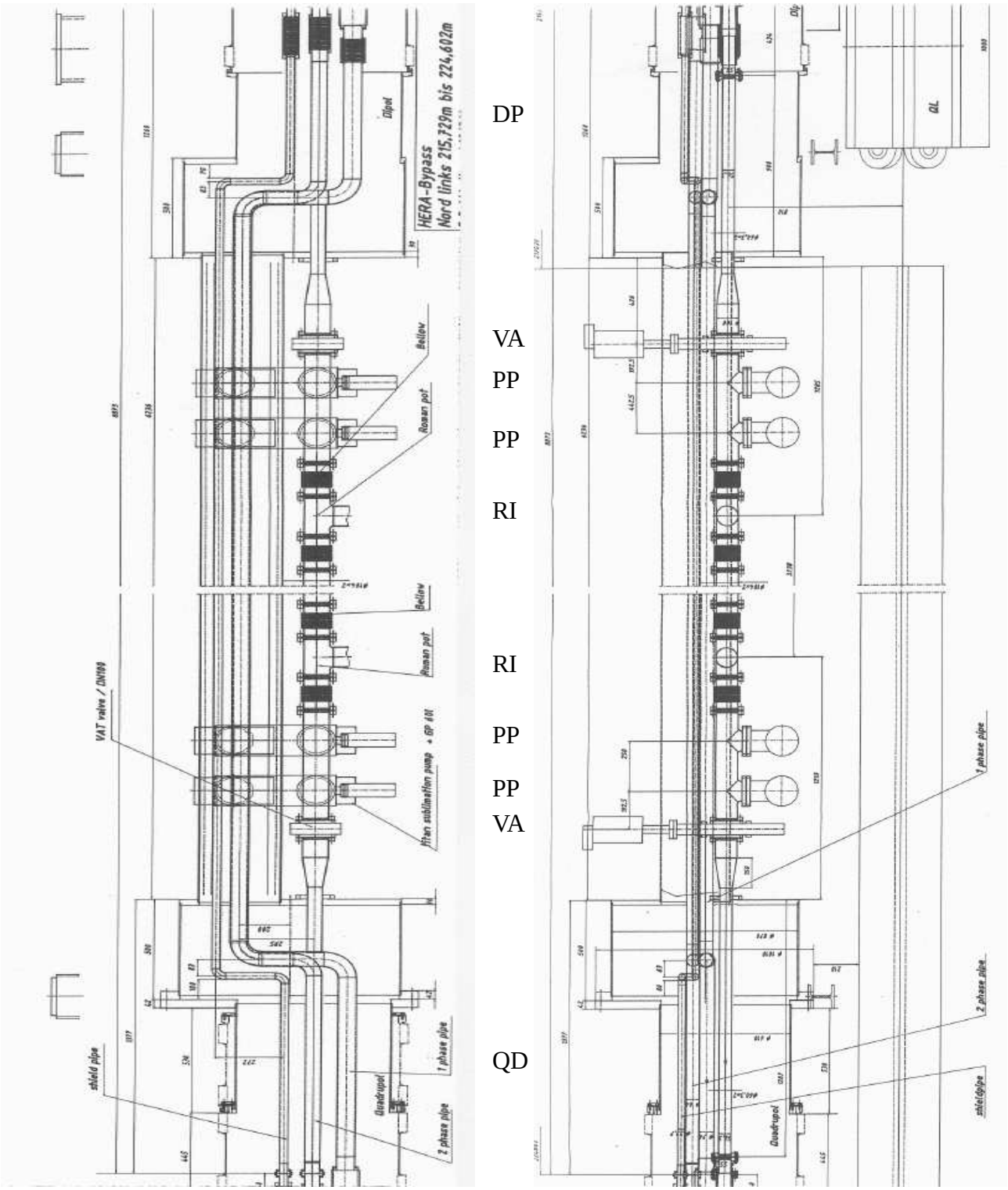

Figure 12: Horizontal and vertical view of the bypass scheme: VA=shutter valves, PP=Titan sublimation pumps, RI=Roman pot inserts, DP=Dipole magnet, QD=Quadrupole magnet, BP=Beam pipe

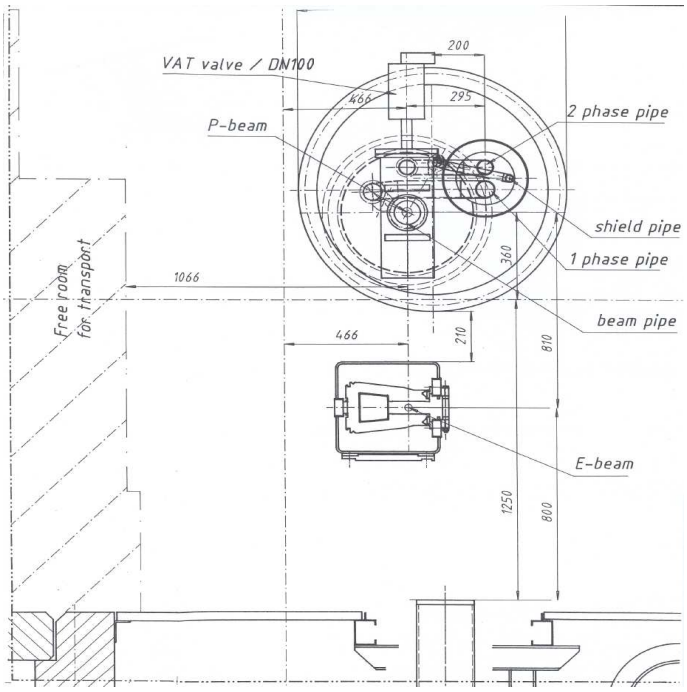

Figure 13: A cross sectional view of the HERA tunnel in the bypass scheme. Indicated are the beam pipe and the bypass with the 1-phase and 2-phase helium lines and the electron beam. The hatched area *Free for Transport* on the left hand side indicates the space occupied by the HERA tunnel transport chariot.

The design of the present H1 Roman pots is completely adequate for housing the new detectors; only the diameter of the T-shaped insert will be reduced to 100 mm. The plunger vessel's movement is guided by four spring loaded guiding rods. The precision of the plunger vessel movement is determined by the precision of a sliding rail. The movement of the electronic box, fixed to the top of the plunger vessel, is controlled by a second moving chariot, which is guided by the same sliding rail. The horizontal advance of the Roman pots is controlled by a stepping motor connected to a hydraulic system. The stepping motor, which is remotely controlled from the H1-control room, has a precision of 5 μm/turn. The measurements of the relative position of the Roman pots with respect to an external reference system (HERA Magnets) is obtained via a measuring probe, the data of which are transmitted via Ethernet to the H1-control room. In the case of a high background rate (or current failure) a fast retraction of the pots is obtained by opening a magnetic valve in the hydraulic system, which releases the hydraulic pressure and results in a fast removal of the Roman pots via the spring loaded guiding rods.

The plunger vessel itself is a stainless steel cylinder with a bottom plate and windows 0.3 mm thick. The thickness is a tradeoff between mechanical stability (vacuum) and the need to keep the multiple scattering of the scattered protons as well as the material in the beam halo to a minimum.

8 The FPS Detector

As mentioned in section 5.3 the coordinates of the impact points of the scattered protons should be measurable with the Roman Pot detectors to a precision of about 100 μm. The data acquisition from these detectors should be operated at the HERA bunch crossing frequency, delivering signals which should preferably be in time to enter the first trigger level L1. From the measured position and angle of the scattered proton, and the knowledge of $x_{I\!P}$ obtained from central detector measurements, the momentum transfer t can be measured. The detector design and construction closely follow the upgraded version of the already existing H1 forward proton spectrometer detectors, which use scintillating fibres.

8.1 General Design

A pictorial view of the T-shape beam insert, plunger vessel, detector and associated electronics for the present H1-FPS is shown in Fig. 14. The new $\mathrm{Roman\ pots}$ will be very similar in design.

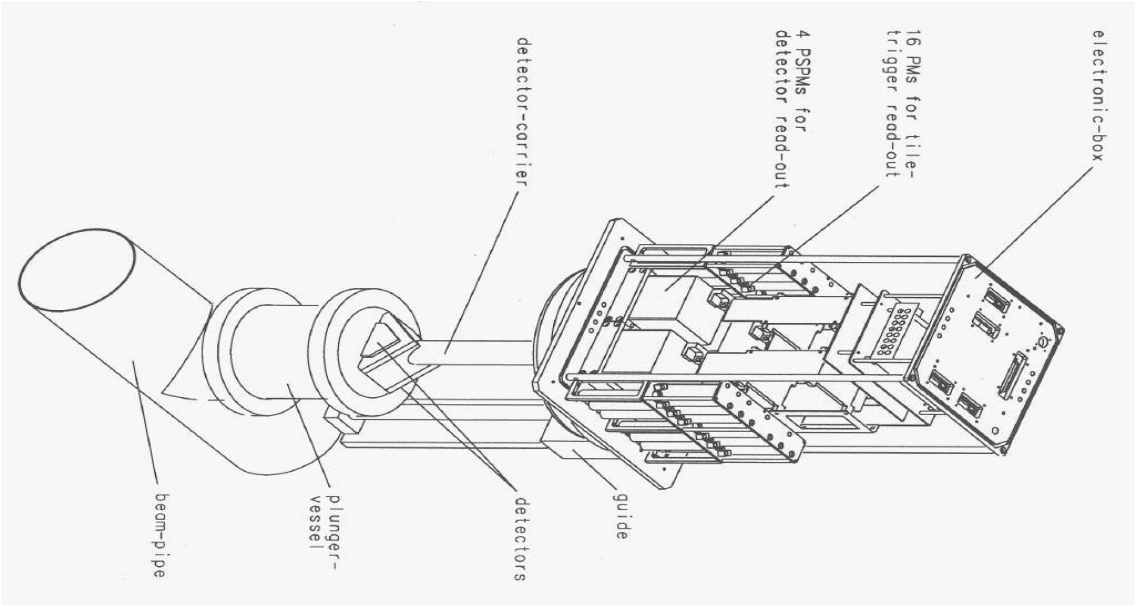

Figure 14: A vertical H1-FPS detector station. For the proposed detectors the two stations will be horizontal.

In Fig. 15 the detector support arm, the electronic box as well as the reference point (ball) for locating the pots with respect to the HERA magnets are shown. A closeup of the 2 scintillating fibre detectors contained in a single Roman Pot is shown in Fig. 15. Notice that this drawing refers to the present FPS detectors; in the VFPS version no finger counters will be present, but one plane of scintillating fibres. Each detector is composed of two u, v planes of scintillating fibres at $\pm 45^0$ with respect to the horizontal pot movement direction and hence measures the position of an incident particle. A subdetector, measuring a single coordinate, is composed of five layers of 62 scintillating fibres as shown in Fig. 16. The even numbered layers are staggered with respect to the odd numbered layers. The five scintillating fibres which are hit by a perfectly perpendicular incident beam are connected to a single light guide via loose plastic connectors,

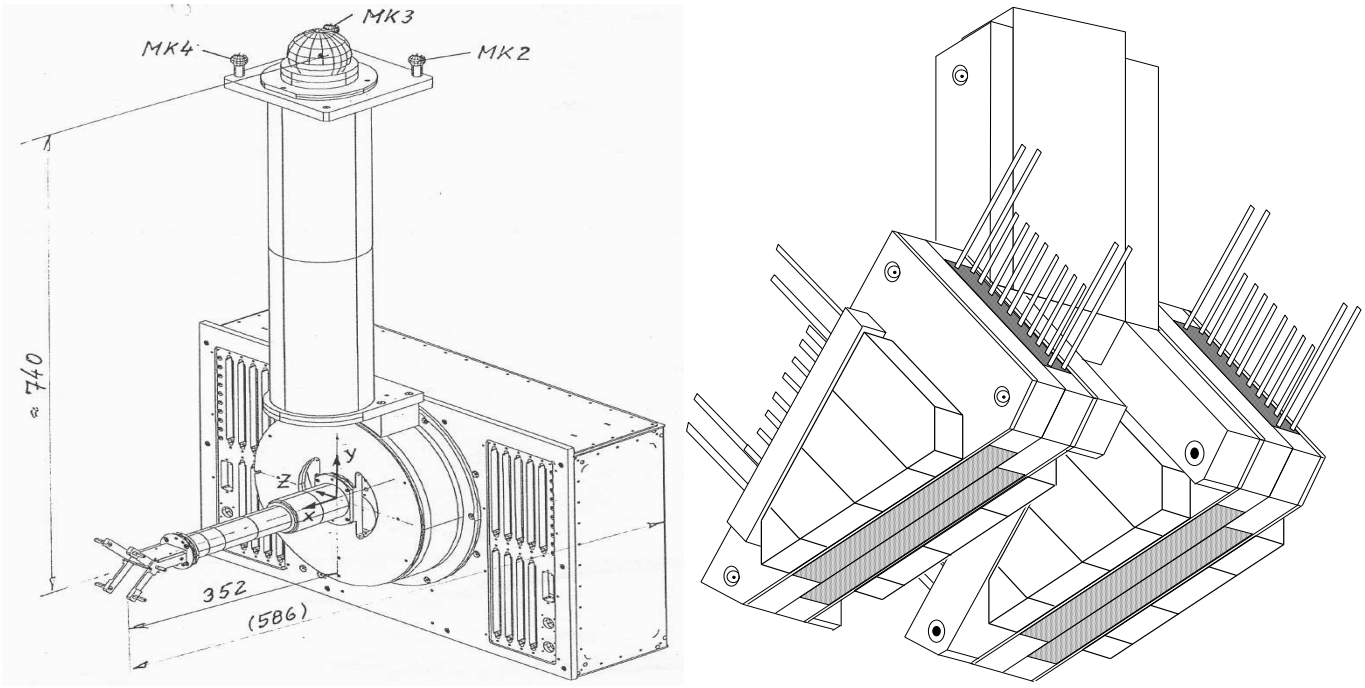

Figure 15: *Left:* The detector support arm (contained in the plunger vessel) and the electronic box connected to it. *Right:* The end of the support arm and the two fibre detectors

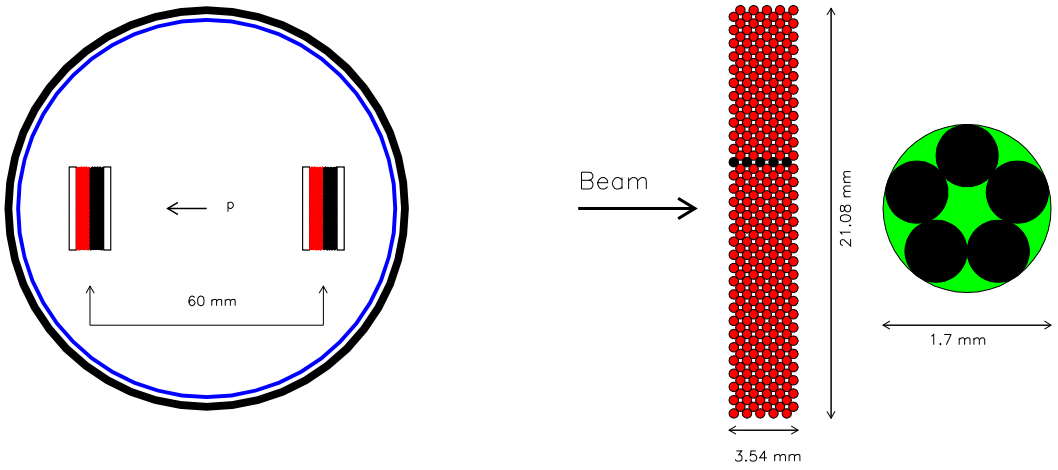

Figure 16: *Left:* The two detectors contained in a Roman Pot. Each detector consists of a u and a v plane sandwiched between two trigger planes. *Right:* A single plane of scintillating fibres with staggered fibres and the arangment of 5 scintillating fibres to be the connected to one light guide.

Detector parameters and results		
	Proposed Detectors	Prototype Detector
fibre $\emptyset$	480μm	480μm
Length fibre	<10 cm	30 cm
Light guide $\emptyset$	1.7 mm	1.7 mm
Length Light guide	500 mm	300 cm
Fibre distance layer	340 μm	340 μm
Detector width ($\perp$-beam)	21.1 mm (62 fibres)	217.6 mm
Detector width ($\parallel$-beam)	3.6 mm (5 layers)	4.76 mm
N-fibres/Light guide	5	7
Fibre material	SCSF-78M(KURARAY)	
PSPM 64 channel	R5900-M64(HAMAMATSU[22])	
	Estimated	Measured
$N_{<pe>}$	8.2	9.4
Detection Efficiency	99.4 %	99.0%
Spatial resolution	94μm	94μm

Table 4: Detector parameters and spatial resolution as proposed for the PS, obtained from results of existing prototype detectors for HERA-B

according to the scheme indicated in Fig. 16. The characteristics of the proposed detector and detector components are summarized in table 4.

The light guides are viewed by a 64-channel position sensitive photomultiplier (PSPM) via a plastic mask corresponding to the anode pixel pattern (2×2 mm^2). There are four PSPM's for each $\mathrm{Roman\ pot}$ station. For triggering purposes each detector is sandwiched between 2 scintillating planes which are connected to different PM's.

8.2 Test Results

Prototype fibre detectors have been constructed by DESY-Zeuthen for HERA-B, with a very similar design to the one proposed, except for the number of fibre layers perpendicular to the beam (see table 4). They were subsequently tested in a 3 GeV electron beam at DESY.

The results obtained from these prototype tests [23] are summarized in table 4. The light attenuation in the light guides was measured to be 6.7 ± 0.7 m. The construction precision, i.e. the precision with which the fibres are positioned within the fibre detector, is of the order of 20μm. Cross talk can be important and reaches 10% at 1 photo-electron (P.E.) level. However analysis has shown that a cut above the 1 P.E. level can be applied as the measured average number of P.E. is 8.2 per road, leading to a detection efficiency of 99.4 %. As a scattered proton can hit more than 1 road because of fibres overlapping and because of the beam divergence, a cluster algorithm has been applied to determine the position of track segments in one detector plane. The positional resolution obtained is 94 μm overall, which is largely sufficient for the present purpose.

This proposed scintillating fibres have been subjected to radiation hardness tests using various beam particles and different radiation doses [24], [25]. The worst case scenario was found in an exposure of a 1 Mrad dose over a period of weeks, which tended to degrade the fibres by at most 30%. All other tests revealed either a complete recovery of the fibres or a marginal degradation of less than 10%.

8.3 Prototype Test

Detectors with specifications as proposed in table 4 have been built as an upgrade for the present FPS detector of H1 and were installed at the end of 1999, replacing one of the existing $\mathrm{Roman\ pot}$ detectors. Analysis of the data in the following months will determine the performance of these detectors in real beam conditions.

8.4 DAQ

The basics of the present FPS-DAQ can also be used for the new pots. This program consists of two main packages, a data acquisition program and a monitor/control package. Although the former could be used as such, the control/monitor package should be updated because of the availability of newer and higher performance PC's and interfaces than those presently in use.

8.5 Roman Pots - Electronics

The concept for the Roman Pot electronics will be the same as for the present FPS detectors. It consists of three main parts:

- detector front end electronics;
- electronics located in the HERA tunnel 10 m from the detector;
- VME Master crate located close to the central trigger logic.

The detector front end electronics comprise the preamplifiers and comparators which, together with the PSPM's and the front end trigger electronics, will be housed in the electronic box mounted on the plunger vessel.

The analog signals from the PSPM's will be transported to a crate located about 10 m from the detector in the HERA tunnel. This crate contains a) the pipeline boards which convert the analog pixel signals via 6-bit FADC's and store the data, b) a trigger board which handles the digital information of the trigger counters, c) a crate controller which controls the pipeline register readout. Communication with the VME master crate in the electronics hut is controlled by the master controller card which sends the data over a bidirectional optical fibre. A detailed description of the FPS electronics can be found in [26].

Several electronic boards constructed for the present FPS exist and can be readily used. Some of them have to be reproduced, while the pipeline board and trigger board, due to longer

signal delay, require a redesign. The VME master crate will be used in the existing FPS configuration.

An important question is whether the VFPS trigger signals can be produced in time for the CTL L1 trigger level. Assuming a fast (4.5 ns/m) cable connection between VFPS and CTL and taking into account the electronic board signal delays [4], it has been estimated that the VFPS trigger signal would arrive with a delay of 1.96 μs and could therefore be used at trigger level L1. Hence the VFPS trigger signal could be used as a deadtime free diffractive trigger.

If, for technical reasons connected to the fast cable connection, the VFPS trigger signal would be too late for L1, then the trigger signal has to enter at level 2. Diffractive events would then be triggered on the basis of electron identification at level 1. Such triggers may have prohibitively high rates so that random downscaling is required, which would reduce the statistics collected by the VFPS.

9 Time Planning - Cost Estimates

9.1 Time planning - Bypass

A complete design of the cold bypass was estimated to take 2 months. The company which was contacted for the mechanical construction of the bypass estimated in their project planning that the complete construction and installation would take about 7 months. A large fraction of this time is related to purchasing material, while 2 months are required for the proper construction of the bypass. The installation will take 1.5 month to which 1 month should be added for the warm up/cool down. In this, the work related to the DESY infrastructure has not been evaluated.

9.2 Overall Time Planning

A first time planning for the design, construction and installation of the cold bypass and of the $\mathrm{Roman\ pot}$ detectors is given in the table below.

The present study indicates that installation of the bypass will take about 6 weeks. This is a major operation as it requires the breaking of the HERA ring vacuum and can only be planned after discussions in close agreement with the different DESY Groups mentioned earlier.

9.3 Cost Estimates

The cost estimates given below regarding the detector construction and related electronics are projections based on estimates from the H1 FPS. The cost estimates regarding the bypass are based on a “Project Design” from one engineering company based on a previously made prestudy of the bypass design, executed by a different engineering office.

[4] Private communication with R. van Staa

Item	Date	Duration(month)
	—2000—	
- Design study of cold bypass	1/6	3
- Construction cold bypass	1/10	7
- Construction warm beam line		-
- Plunger Vessel design		-
- Adaptation of DAQ + trigger		-
- Radiation tests at Roman pot location		-
	—2001—	
- Plunger Vessel Construction		4
- Detector Construction		3
- Bypass Installation (shutdown 2001-2002) (including warm up/cool down)		2.5
	—2002—	
- Roman pots Installed/Testing		
- DAQ-trigger Installed/Testing		
	—2003—	
- Tests / Data Taking		
	—2004—	
- Data Taking		

Table 5: Time planning

Item	Cost(in kDM)	number	Total Cost
- Bypass : Design study	150	1	150
- Bypass : Construction/transportation/ installation at DESY	320	1	320
- Bypass : installation in DESY infrastructure	25	1	25
- Warm beam pipe, pumps + shutters	200	1	200
- Roman Pot mechanics (plunger Vessel) + stage control	50	2	100
- Detector Mechanics + front end electronics (Mechanics + Trigger + PM + PSPM)	50	2	100
- Detector Electronics	100	2	200
- DAQ/Trigger VME	100	1	100
Total			$\approx$ 1.200

Table 6: Cost estimates

Item	Institute
- Fibre detectors	Zeuthen(construction)
- Roman pot plunger	Antwerp/Brussels
- Detector front end electronics	Hamburg II
- DAQ + trigger	Lund
- Bypass/beam pipe installation	Antwerp/Brussels
- Software	All

Table 7: Group interests

9.4 Interested Groups

The present project is supported by the groups of Antwerp, Brussels, Birmingham, Hamburg II and Lund. They will contribute to the project according to the table below. In addition, the Zeuthen group (J. Baehr) stated that they are prepared to construct the optical fibre detectors and are willing to share their know how. In order to get acquainted with the Roman Pot detectors we have joined them in the test runs concerning the FPS upgrade in 1999/2000.

The interest of the different groups regarding the technical aspects of the experiment are summarized in the table below.

Acknowledgements

In writing this proposal we very much profitted from the information and the experience from all the people who built and operated the H1 FPS detector. In particular we would like to mention W. Bartel, M. Seidel and J. Baehr.

The idea of the construction of a cold bypass resulted from many discussions with the DESY Cryogenics Group, in particular S. Wolff, G. Hoffman and H. Lierl. Also the information from and discussion with the DESY Vacuum Group, in particular K. Zapfe and D. Huber were very important. Without the cooperation and support of all these people the cold bypass idea would not have become a realistic solution for installing Roman pots into the proton beam line. Their cooperation and support in the future will be of the utmost importance.

Many elucidating discussions with many people have preceded the writing of the present proposal. We would like to thank in particular F. Willeke, B. Holzer, C. Eggert, V. Avati, M. Arneodo and J. Whitmore.

We also appreciate the encouragement of our spokesmen and the whole of the H1 diffractive group especially W. Bartel and R. Felst.

References

[1] *ep* Physics beyond 1999, H1 internal report H1-10/97-531;
The HERA Luminosity Upgrade, ed. U. Schneekloth, DESY HERA 98-05 (1998).

[2] ZEUS Collab., J. Breitweg et al., *Eur. Phys. J.* **C6** (1999) 43.

[3] H1 Collab., C. Adloff et al., *Zeit. Phys.* **C76** (1997) 613.

[4] H1 Collab., C. Adloff et al., *Eur. Phys. J.* **C1** (1998) 495.

[5] ZEUS Collab., J. Breitweg et al., *Phys. Lett.* **B421** (1998) 368.

[6] H1 Collab., C. Adloff et al., *Eur. Phys. J.* **C5** (1998) 439.

[7] H1 Collab., C. Adloff et al., *Phys. Lett.* **B428** (1998) 206.

[8] ZEUS Collab., J. Breitweg et al., *Eur. Phys. J.* **C5** (1998) 41.

[9] H1 Collab., C. Adloff et al., *Eur. Phys. J.* **C6** (1999) 421.

[10] S. Hengstmann, Deep Inelastic Scattering and QCD, 7^{th} International Workshop 1999, Nucl. Phys. B – Proc. Sup., **Vol. 79** (1999) 296

[11] J. Cole, Deep Inelastic Scattering and QCD, 7^{th} International Workshop 1999, Nucl. Phys. B – Proc. Sup., **Vol. 79** (1999) 299

[12] J. Bartels, J. Ellis, H. Kowalski and M. Wüsthoff, *Eur. Phys. J.* **C7** (1999) 443.

[13] M.F. McDermott and G. Briskin, Proc. of the Workshop on "Future Physics at HERA", ed. G. Ingelman, A. De Roeck and R. Klanner, DESY, Hamburg (1996) 691.

[14] N.N. Nikolaev and B.G. Zakharov, Deep Inelastic Scattering and QCD, 5^{th} International Workshop 1997, AIP Conference Proceedings 407, 445.

[15] see e.g. J. Bartels, H. Lotter and M. Wüsthoff, *Phys. Lett.* **B379** (1996) 239;
W. Buchmüller, M.F. McDermott and A. Hebecker, *Phys. Lett.* **B410** (1997) 304.

[16] J. Bjorken, *Phys. Rev.* **D47** (1993) 101;
E. Gostman, E. Levin and U. Maor, *Phys. Lett.* **B309** (1993) 199.

[17] see e.g. L. Alvero, J.C. Collins, J. Terron and J.J. Whitmore, *Phys. Rev.* **D59** (1999) 74022.

[18] J. Bartels, C. Ewerz, H. Lotter, M. Wüsthoff, M. Diehl, Proc. of the Workshop on "Future Physics at HERA", ed. G. Ingelman, A. De Roeck and R. Klanner, DESY, Hamburg (1996) 668.

[19] B. Holzer, Private communication.

[20] Proposal for a Forward Spectrometer for H1, H1-internal report H1-10/94-381.

[21] Upgrade of the H1 Forward Spectrometer, H1-internal report H1-12/95-467.

[22] Y. Yoshizawa et al., Hamamatsu technical information, No. TPMH 9002e01.

[23] Test run results from prototype fiber detectors for high rate particle tracking, NIM **A 424** (1999) 459-469.

[24] E.C. Aschenauer et al., Measurements of the radiation hardness of selected scintillating and light guide fiber materials, preprint DESY 99-078.

[25] J. Bähr et al., A Fiber Detector Radiation Hardness Test, preprint DESY 99-079.

[26] K. Geske, H. Riege, J. Schütt,R. van Staa, H1 Forward Proton Spectrometer Electronics, internal communication of II. Institute für Experimental physik, Universität Hamburg , Juni 1995